Mon. Not. R. Astron. Soc. **273,** 47–58 (1995)

Neutral carbon far-red forbidden line emission from planetary nebulae

X.-W. Liu,[1] M. J. Barlow,[1] I. J. Danziger[2] and R. E. S. Clegg[3]

[1] *Department of Physics and Astronomy, University College London, Gower Street, London WC1E 6BT*
[2] *European Southern Observatory, Karl-Schwarzschild Str., D-85748 Garching bei München, Germany*
[3] *Royal Greenwich Observatory, Madingley Road, Cambridge CB3 0EZ*

Accepted 1994 September 28. Received 1994 September 28; in original form 1994 June 6

ABSTRACT

The temperature-sensitive neutral carbon forbidden lines at 8727, 9824 and 9850 Å have been measured simultaneously for the first time from a planetary nebula. The nebulae NGC 2346, NGC 2440, NGC 3132 and IC 4406 were observed. Accurate rest wavelengths of these lines are obtained. The observed line ratios $I(\lambda 9824+\lambda 9850)/I(\lambda 8727)$ are consistent with collisional excitation by electron impacts. It is demonstrated that radiative recombination and stellar continuum fluorescence are unimportant in exciting the observed [C I] lines, with the possible exception of NGC 2440 where a contribution from the former process cannot be ruled out. For NGC 2346, NGC 3132 and IC 4406, the observed [C I] line ratios yield electron temperatures between 7400 and 8000 K, about 1800 to 2800 K lower than those deduced from the [N II], [S III] and [O III] line ratios that we also measured. Electron densities are derived from the observed [N I], [S II] and [Cl III] doublet ratios.

Key words: line formation – planetary nebulae: general.

1 INTRODUCTION

CO and H_2 observations reveal that many planetary nebulae (PNe) are surrounded by envelopes of neutral gas, whose masses often greatly exceed those of the ionized nebulae (Huggins 1993). Although IR and mm-wave molecular observations have provided important information on the structure and kinematics of the envelopes, details about the chemistry and origin of molecules in this important component of PNe remain unknown. This unsatisfactory situation is partly due to our lack of knowledge concerning the physical and chemical conditions prevailing in these regions. In particular, there are still no direct measurements of fundamental parameters such as density and kinetic temperature, partly due to a lack of suitable diagnostics in the IR.

Here we present long-slit spectrophotometry of three forbidden lines arising from the ground electron configuration of $2p^2$ of neutral carbon, [C I] $\lambda\lambda$8727, 9824 and 9850, emitted by four PNe previously known to show strong molecular hydrogen emission. The ionization potential of C^0 is only 11.26 eV, so it can be ionized by stellar radiation between 912 and 1101 Å penetrating past the ionized region. Radiation of nearly the same energy range photodissociates H_2. Thus C^0 is expected to co-exist mainly with H_2, making it an invaluable probe of the H_2-emitting regions. [C I] $\lambda\lambda$9824, 9850 emission was first identified in NGC 7027 (Danziger & Goad 1973). Jewitt et al. (1983) searched for [C I] emission from six PNe, and detected the $\lambda\lambda$9824, 9850 lines in the spectra of three of them. These [C I] lines have also been observed from photodissociation regions (PDRs) around the H II regions M 42 (Hippelein & Münch 1978) and NGC 2024 (Münch & Hippelein 1982). More recently, Burton et al. (1992) detected strong [C I] λ8727 emission from the PDR of the reflection nebula NGC 2023. Modelling calculations by Escalante, Sternberg & Dalgarno (1991) of the thermal structure and chemistry of PDRs show that for M 42 and NGC 2024 the observed [C I] far-red emission must arise mainly from radiative recombination of C^+ ions produced by photoionization. However, the [C I] forbidden lines observed in PNe appear to have a different origin, i.e. collisional excitation by electron impacts (Danziger & Goad 1973; Jewitt et al. 1983). The dominant excitation mechanism of [C I] lines can, however, be easily established by simultaneously measuring the λ8727 and $\lambda\lambda$9824, 9850 lines of [C I].

Since C^0 has the same ground electron configuration as O^{2+}, under the condition of collisional excitation the forbidden line ratio [C I] $(\lambda 9824+\lambda 9850)/\lambda 8727$, like [O III] $(\lambda 4959+\lambda 5007)/\lambda 4363$, is a sensitive temperature probe. Such measurements, presented here, can potentially provide a direct measurement of the electron temperature in the warm neutral transition regions around PNe.

In addition to the [C I] lines, we have also measured the [N I] doublet ratio $\lambda 5200.42/\lambda 5197.95$, which is one of the very few density-sensitive diagnostics observable from a neutral species in the optical region. (Another potential diagnostic is the Mg I] intercombination line ratio $\lambda 4562/\lambda 4571$,

which has been used by Clegg et al. (1987) to derive an electron density of about 9500 cm^{-3} for NGC 3918. The Mg I] lines are, however, very weak and difficult to observe in most PNe.)

2 OBSERVATIONS AND DATA REDUCTION

The data reported here were secured in 1994 February using the ESO 1.52-m telescope with the Boller & Chivens spectrograph and a Ford 2048 × 2048 (15-μm pixel) CCD. A journal of observations is given in Table 1. A 1200 groove mm^{-1} grating in first order was used to cover the 8010–9980 Å wavelength region at a resolution of 2 Å (FWHM). An RG715 filter was used to block light from the second order. Each pixel along the slit projected to 0.81 arcsec on the sky. The *HST* standard star HD 49798 (Oke 1990) was observed with a slit width of 6 arcsec for flux-calibration purposes. The 5023–7007 Å wavelength region was observed with another 1200 groove mm^{-1} grating in first order, providing a resolution of 2 Å (FWHM). A GG475 filter was used to cut out light from the second order. The standard stars HD 49798 (Oke 1990; Walsh 1993) and L745-46A (Oke 1974) were observed for calibration purposes. Due to the demagnification by the Boller & Chivens spectrograph at large grating angles, the spectral line profiles were slightly undersampled. Throughout the observations, identical slit positions were used for the two grating settings for each PN.

All the data were reduced in the standard way for long-slit spectra using IRAF running on a Starlink DEC-station at UCL. The spectra were bias-subtracted, flat-fielded and wavelength-calibrated via exposures of a helium-argon lamp. The dark current of the Ford CCD is negligible, less than $2\,e^-$ $pixel^{-1}$ h^{-1}; thus no dark current was subtracted. The sky background was subtracted by fitting a low-order polynomial column by column to scan lines outside the nebular emission. The geometric distortion of the CCD spectra was negligible. Even though the far-red wavelength is crowded by strong sky OH emission, accurate sky subtraction has been achieved. The three [C I] lines that we are interested in are not affected by any nearby sky OH emission lines (Osterbrock & Martel 1992).

Parts of the far-red wavelength region are seriously affected by telluric absorption lines. Fortunately, unlike the wavelength region between 9000 and 9800 Å, where numerous telluric absorption lines are crowded together and can distort observed spectra, the three [C I] lines lie in regions with relatively sparse telluric absorption lines (e.g. Delbouille & Roland 1963; see also Section 3 for details on the possible effects of telluric absorption on individual [C I] lines). In deriving instrumental monochromatic response, we have carefully deleted calibration points affected by telluric absorption and then fitted the remaining points by a smooth curve. We estimate that an accuracy of 5 per cent in relative flux calibration has been achieved.

The spectra were corrected for interstellar extinction using the reddening curve of Seaton (1979). For NGC 2346 and 3132, spectra covering the λλ3570–7400 region at a resolution of 3.5 Å (FWHM) were also obtained in the same observing run. These data will be presented in a separate paper. For these two objects, values of the logarithmic extinction at Hβ, $c(H\beta)$, deduced from these low-resolution data by comparing the observed Balmer decrement with values predicted by case B recombination theory (Hummer & Storey 1987) have been used, and are equal to 0.22 and 0.06 for NGC 2346 and 3132, respectively. For NGC 2440, we have adopted $c(H\beta)=0.44$, derived by Liu & Danziger (1993) from the Balmer decrement. For IC 4406, we use $c(H\beta)=0.28$, derived by Torres-Peimbert & Peimbert (1977). Plots showing the observed [C I] lines in the spectra of IC 4406 and NGC 2440 are given in Fig. 1.

3 RESULTS

3.1 Wavelengths of the far-red [C I] forbidden lines

The rest wavelengths of the [C I] forbidden lines λλ8727 and 9850 were measured previously by Swensson (1967; cf. the compilation by Kaufman & Sugar 1986) by tracing the solar spectrum of Delbouille & Roland (1963). A better wavelength determination for the λ8727 line was given by Lambert & Swings (1967), 8727.13 ± 0.02 Å, using a high-resolution solar scan recorded at the Kitt Peak Observatory. Lambert & Swings also found evidence of the [C I] transauroral line λ4622 in the solar spectrum. Although the solar [C I] λ8727 line is reasonably strong and its wavelength well determined, the solar λ9850 line is weak and difficult to measure. The λ9824 line has not been measured in the solar spectrum, being probably lost in the telluric absorption

Table 1. Observational journal.

Object	Date (UT)	Exposure Time (sec)	Wavelength (Å)	FWHM (Å)	Slit-width (arcsec)	PA (degree)
NGC 2346	94/02/04	4 × 1800	8010–9980	2	2	70
	94/02/05	300,4 × 1800	5023–7007	2	2	70
NGC 2440	94/02/04	2 × 1800	8010–9980	2	2	158
	94/02/05	120,4 × 600	5023–7007	2	2	158
NGC 3132	94/02/04	3 × 1800	8010–9980	2	2	72
	94/02/05	300,2 × 1800	5023–7007	2	2	72
IC 4406	94/02/04	3 × 1800	8010–9980	2	2	172
	94/02/05	600,2 × 1800	5023–7007	2	2	172

Slit position: NGC 2346 through the central star; NGC 2440 through the centres of the two [O I] λ6300 emission peaks as mapped by Reay, Walton & Atherton (1988); NGC 3132 through the central star; IC 4406 through the apparent centre.

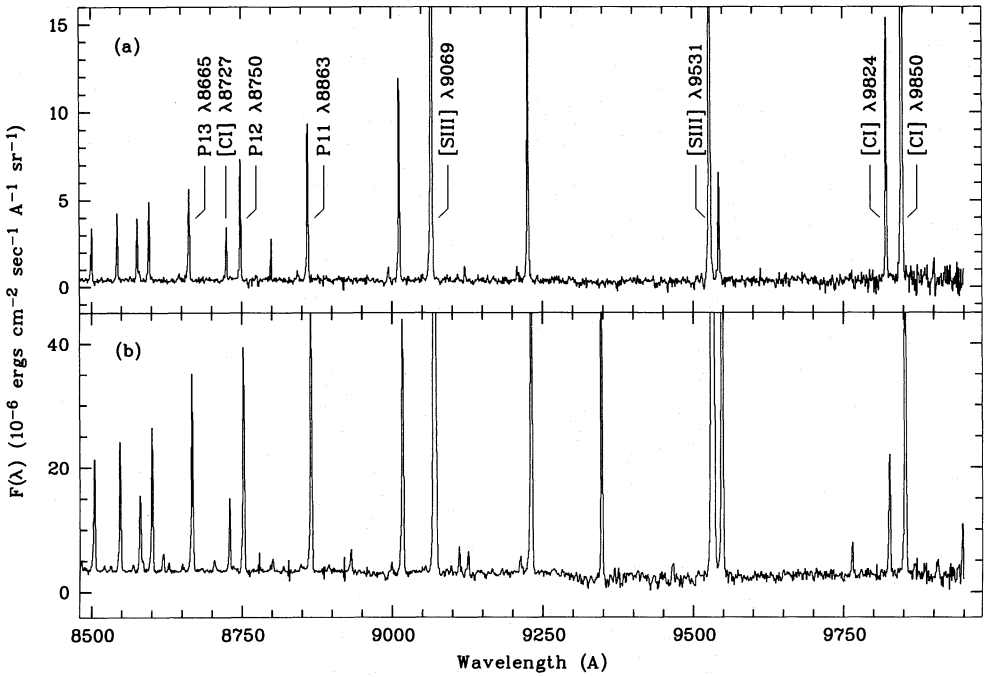

Figure 1. Far-red spectra of (a) IC 4406 and (b) NGC 2440, showing the [C I] forbidden lines. Correction has been made for interstellar reddening.

features. With the spectral resolution used here, the standard deviation of the residuals in wavelength of our wavelength calibration was about 0.05 Å, which makes a better wavelength determination possible for the latter two [C I] lines.

To derive the rest wavelengths from the observed ones, we need to know the radial velocities of the nebulae observed. Recent measurements of heliocentric radial velocities for nebulae studied here are given by Meatheringham, Wood & Faulkner (1988), who observed the He II λ4686, [O III] λ5007 and [O II] λλ3726, 3729 lines using a slit echelle spectrograph. They found +20, +63, −10 and −41 km s^{-1} for NGC 2346, NGC 2440, NGC 3132 and IC 4406, respectively. These are claimed to be accurate to 2–3 km s^{-1}. However, a subtle point in nebular velocity measurement is that PNe are typically expanding at speeds of 10–20 km s^{-1} and exhibit velocity differences of this order at various points in the nebula (Schneider et al. 1983). In slit observations of extended nebulae such as those studied here, only a small fraction of the total flux emitted by the nebula is caught by the narrow slit. Thus radial velocities derived from this kind of observation may depend on the actual slit positions used. Radial velocities derived from different lines may differ as well, as lines of different excitation energy arise from different parts of the nebula. For accurate wavelength measurements, it is therefore preferable to use radial velocities derived from lines of similar excitation energy, and to observe them at identical slit positions. For this purpose, we have derived the heliocentric radial velocities using the *nebular* [O I] lines at 6300 and 6363 Å, which are likely to arise from similar nebular regions to the [C I] lines of interest here. The rest wavelengths of the [O I] lines are accurately known, 6300.304 ± 0.002 and 6363.782 ± 0.002 Å, respectively (Kaufman & Sugar 1986). For all four of the objects observed here, the radial velocities derived from the two lines agree within 1.5 km s^{-1}. Given the fact that the λ6300 line is about three times stronger than the λ6363 line, we thus average the velocities deduced from them with weights of 3 and 1, respectively. The results are heliocentric radial velocities of +30.15, +54.52, −13.57 and −46.70 km s^{-1} for NGC 2346, NC 2440, NGC 3132 and IC 4406, respectively (as a check of the wavelength calibration, the mean rest air wavelengths derived for the *sky* [O I] lines in the spectra of the four nebulae are 6300.28 ± 0.02 and 6363.788 ± 0.02 Å, respectively, in agreement within the errors with those given by Kaufman & Sugar 1986). We also measured the heliocentric radial velocities of the hydrogen P11 line at 8862.787 Å, P12 at 8750.475 Å and P13 at 8665.021 Å (Moore 1972). These lines bracket in wavelength the [C I] λ8727 line, and are clear of telluric absorption. They give heliocentric radial velocities of +26.4 ± 0.8, +54.4 ± 0.5, −15.0 ± 0.1 and −50.2 ± 0.4 km s^{-1} for the four nebulae, in the above order. The velocities derived from the hydrogen Paschen lines generally agree quite well with those deduced from the [O I] nebular lines. Our radial velocities, however, differ significantly from those of Meatheringham et al. (1988), probably due to the different slit positions and lines used. However, from multiple-slit observations, Walsh (1983; see also Walsh, Meaburn & Whitehead 1991) deduced a heliocentric velocity of +28 km s^{-1} for NGC 2346 from observations of the [N II] λ6584 line, which is in better agreement with the results given here.

The final rest wavelengths deduced for the [C I] lines are given in Table 2. Our own radial velocities deduced from the nebular [O I] lines have been used for the reasons described above. The wavelengths deduced from the spectra of the four objects agree quite well, confirming the validity of the radial velocities adopted and the accuracy of the wavelength calibration. The average wavelength derived for the λ8727 line

is in excellent agreement with that of Lambert & Swings (1967). The new wavelength derived for the λ9850 line should be more reliable than that of Swensson (1967). The new wavelengths derived for the $\lambda\lambda$9824, 9850 lines, however, differ significantly from the theoretical values listed in Kaufman & Sugar (1986). Since the $\lambda\lambda$9824, 9850 lines fell towards the end of our spectra, as a check on possible systematic error in wavelength calibration near this wavelength region, we have measured the wavelength of the OH sky emission line 3–0 $P_1(2)$ at 9872.14 Å (Osterbrock & Martel 1992), a strong, isolated sky emission line close by in wavelength to the [C I] $\lambda\lambda$9824, 9850 lines. The mean wavelength deduced from the spectra of the four nebulae is 9872.125 ± 0.003 Å. We therefore believe that our new wavelengths for the $\lambda\lambda$9824, 9850 lines should be reliable. As we will show below, for three out of the four nebulae observed here, the λ9824 line is possibly affected by telluric absorption lines, which would explain the relatively large standard error in rest wavelength found for this line.

Table 2. Rest air wavelengths of far-red forbidden lines from the ground electron configuration $2p^2$ of neutral carbon.

	Transition		
	$^1S_0 - {}^1D_2$	$^1D_2 - {}^3P_1$	$^1D_2 - {}^3P_2$
NGC 2346	8727.17	9824.42	9850.37
NGC 2440	8727.14	9824.36	9850.36
NGC 3132	8727.07	9824.21	9850.32
IC 4406	8727.08	9824.23	9850.37
mean	8727.12 ±0.02	9824.30 ±0.05	9850.36 ±0.01
Swensson[a]	8727.18 ±0.10		9850.28 ±0.10
Lambert & Swings[b]	8727.13 ±0.02		
Calculated[c]	8727.141 ±0.022	9824.109 ±0.022	9850.243 ±0.022

[a]Observed wavelengths from Swensson (1967). The error bars are quoted from Kaufman & Sugar (1986).
[b]Observed wavelength from Lambert & Swings (1967).
[c]Kaufman & Sugar (1986).

3.2 The fluxes of the far-red [C I] forbidden lines

The observed surface brightnesses of the three [C I] lines and of P11, the strongest H I recombination line clear of telluric absorption in this wavelength region, along with their intensities in units where $H\beta = 100$ (normalized via P11), after correcting for interstellar reddening, are given in Table 3. They were measured on integrated spectra, summed over all scan lines where the [C I] emission was detected. For the same object, line fluxes measured on consecutive individual spectra are in excellent agreement. The integration areas along the slit for each nebula are described in the notes to Table 3. For each object, the same integration areas are used for spectra covering the $\lambda\lambda$5023–7007 wavelength region. The intensity of hydrogen P11 relative to $H\beta = 100$ was taken from Hummer & Storey (1987) using the nebular temperatures and densities listed in Table 4 (Section 3.3); values of 1.35 for NGC 2440 and 1.38 for the other three nebulae were adopted. The wavelengths of the [C I] lines in the reference frame of Earth at the time of observation, $\lambda^{\rm Earth}$, are also listed in Table 3. They are used to check for possible absorption of the [C I] lines by telluric absorption lines. Instead of using the apparent wavelengths from individual objects, the mean rest wavelengths of [C I] lines derived in Table 2 were adopted, as they should be more accurate, and then converted to the Earth reference frame using the heliocentric radial velocities deduced from the nebular [O I] lines given in Section 3.1.

Whereas P11 and [C I] λ8727 are clear of telluric absorption, there are several water vapour absorption lines near [C I] $\lambda\lambda$9824, 9850. Their effects on the observed line fluxes change from object to object, depending on the radial, expansion and thermal velocities of the nebula as well as turbulent velocities, if significant. The telluric absorption lines cannot be resolved at our spectral resolution, and it is very difficult to correct for their effects (see, e.g., Stevenson 1994). We assume that a measurement can be affected by telluric absorption significantly if there are one or more tel-

Table 3. Dereddened line fluxes.[a]

Line	NGC 2346			NGC 2440			NGC 3132			IC 4406		
	$\lambda^{\rm Earth}$	$S(\lambda)^b$	$I(\lambda)^c$	$\lambda^{\rm Earth}$	$S(\lambda)^b$	$I(\lambda)^c$	$\lambda^{\rm Earth}$	$S(\lambda)^b$	$I(\lambda)^c$	$\lambda^{\rm Earth}$	$S(\lambda)^b$	$I(\lambda)^c$
H I P11	8863.73	3.45	1.38	8864.80	155	1.35	8862.11	13.4	1.38	8860.79	23.9	1.38
[C I] λ8727	8728.40	2.00	.800	8728.91	32.0	.279	8726.26	4.86	.500	8724.96	6.81	.393
[C I] λ9824	9825.73	14.3:	5.72:	9826.30	64.8:	.564:	9823.32	37.0	3.81	9821.86	40.0:	2.31:
[C I] λ9850	9851.81	50.3	20.1	9852.38	228.	1.98	9849.39	113.:	16.3:	9847.93	138.	7.97
R^d		33.6			9.53			30.1			27.1	

[a]Fluxes are measured on spectra integrated along the slit. Integration slit lengths are: NGC 2346, 46.74 arcsec centred on the central star excluding the central 9.02 arcsec; NGC 2440, 26.24 arcsec centred on the apparent nebular centre; NGC 3132, 50.02 arcsec centred on the central star excluding the central 26.24 arcsec; IC 4406, 34.44 arcsec centred on the central star. The slit width is 2 arcsec in all cases. Measurements possibly affected by telluric absorption are marked by a colon. See text for details.
[b]Surface brightness in units of 10^{-6} erg cm^{-2} s^{-1} sr^{-1}.
[c]Intensity in units of $H\beta = 100$.
[d]$R \equiv I(\lambda9824 + \lambda9850)/I(\lambda8727)$. In calculating R, only one of the λ9824 and λ9850 lines is used, depending on which is clear of telluric absorption. The other line, affected by telluric absorption, is then incorporated assuming $I(\lambda9850)/I(\lambda9824) = 2.96$, as derived from the transition probabilities given by Nussbaumer & Rusca (1979).

Table 4. Plasma diagnostics.[a]

Diagnostics	NGC 2346	NGC 2440	NGC 3132	IC 4406
		N_e (cm^{-3})		
[N I] λ5200/λ5198	700(.924)	3400(.652)	860(.887)	1330(.793)
[S II] λ6716/λ6731	270(1.18)	1900(.722)	660(.961)	930(.878)
[Cl III] λ5517/λ5537	850(1.20)	4950(.744)	900(1.18)	720(1.23)
		T_e (K)		
[C I] (λ9824+λ9850)/λ8727[b]	7440(33.6)	14950(9.53)	7800(30.1)	8020(27.1)
[N II] (λ6548+λ6584)/λ5755	10270(82.7)	10360(79.8)	9800(92.9)	10120(85.6)
[S III] (λ9069+λ9531)/λ6312	9150(79.8)	15640(27.2)	9560(71.3)	10360(58.6)
[O III] (λ4959+λ5007)/λ4363	9930(217.)	14200(80.1)[c]	9590(244.)	10560(178.)[d]

[a]Numbers in parentheses are the corresponding diagnostic line intensity ratios.
[b]Section 4.3.
[c]Liu & Danziger (1993).
[d]Torres-Peimbert & Peimbert (1977).

luric absorption lines with central optical depths in excess of 0.2, as seen on the solar spectrum atlas of Delbouille & Roland (1963), falling within the wavelength range $\lambda^{\rm Earth}(1-\Delta V/c)$ to $\lambda^{\rm Earth}(1+\Delta V/c)$, where $\lambda^{\rm Earth}$ is the wavelength in the Earth reference frame of the line of interest, $\Delta V = V_{\rm exp} + V_{\rm D}$ is the sum of the nebular expansion velocity and thermal Doppler width, and c is the velocity of light. For $T_e = 10^4$ K, $V_{\rm D} = 3.7$ km s^{-1} for carbon. For NGC 2440, NGC 3132 and IC 4406 we have adopted the [O II] expansion velocities $V_{\rm exp}$ of 33.0, 21.0 and 14.0 km s^{-1}, respectively, from Meatheringham et al. (1988). For NGC 2346 Meatheringham et al. give an expansion velocity less than 6 km s^{-1}. Here we have used 12 km s^{-1}, as estimated from observations by Walsh (1983) and Walsh et al. (1991). The rest wavelengths of telluric absorption lines are taken from Swensson et al. (1970). Line measurements that are possibly affected by telluric absorption are marked by a colon in Table 3.

The [C I] λλ9850, 9824 lines decay from the same upper level, so their intensity ratio depends only on the relative transition probabilities. Using the transition probabilities calculated by Nussbaumer & Rusca (1979), we obtain $I(\lambda 9850)/I(\lambda 9824) = 2.96$. It would be of great interest if this ratio could be measured directly from observations and thus provide a check on the accuracy of the theoretical calculations. Unfortunately, of the four objects observed here, none is clear of telluric absorption for both lines. We have thus adopted the theoretical flux ratio of 2.96 and used only the line that is clear of telluric absorption to calculate the [C I] nebular to auroral line ratio $R \equiv I(\lambda 9824 + \lambda 9850)/I(\lambda 8727)$. The results are listed in Table 3.

3.3 Plasma diagnostics

Nebular properties derived from some of the standard plasma diagnostic ratios are given in Table 4 (the diagnostic line intensity ratios are given in parentheses). They were deduced by solving population equilibrium equations for a multilevel (usually six-level) atomic model. The atomic data used are the same as in Liu & Danziger (1993), except for [N II] where new collision strengths calculated by Stafford et al. (1994) are adopted which give electron temperatures 300–400 K lower as compared to those deduced from atomic parameters of Mendoza (1983). For NGC 2346 and 3132 the [O III] electron temperatures were deduced from our low-resolution spectra described in Section 2. For NGC 2440 and IC 4406 they were taken from Liu & Danziger (1993) and Torres-Peimbert & Peimbert (1977), respectively. The interpretation of the [C I] lines and the validity of their ratio as a temperature diagnostic are discussed in detail in the next section.

The [S III] nebular lines at 9068.9 and 9531.1 Å and the auroral line at 6312.1 Å were covered by our observations. The electron temperatures deduced from the [S III] $(\lambda 9069 + \lambda 9531)/\lambda 6312$ ratio are listed in Table 4. Details of the [S III] temperature determination are given in Appendix A. In addition to uncertainties introduced by telluric absorption lines, as discussed in Appendix A, significant errors can also be introduced to the electron temperatures deduced from the [S III] nebular-to-auroral line ratio through reddening correction, owing to the large wavelength range of the lines involved. For example, the difference between the reddening constant $f(\lambda)$ at λ6312 and at λ9069 is 0.302, as compared with the corresponding value of 0.158 between the [O III] λ4363 and λ5007 lines.

NGC 2440 shows extraordinarily strong [O I] emission. After accurate sky subtraction, the nebular [O I] λ5577 line, which is blended with strong sky emission from the same line, is well detected and measured. The derived [O I] line ratio $I(\lambda 6300 + \lambda 6363)/I(\lambda 5577) = 106$ implies an electron temperature of 9830 K, in good agreement with the value of 10 400 K derived from their observations by Richer, McCall & Martin (1991).

At a spectral resolution of about 2 Å FWHM, the [N I] λλ5197.95, 5200.41 doublet was partially resolved, and the relative line intensities were retrieved by fitting the line profiles with two Gaussians of the same width. The difference in the central wavelengths of the two Gaussians was fixed at 2.46 Å, the difference in their rest wavelengths. The ionization potential of N^0 (14.534 eV) is only slightly larger than that of H^0 and, due to a large charge-transfer reaction rate (Dalgarno 1978; Butler & Dalgarno 1979), N^0 is expected to be abundant in the warm transition region between the neutral envelope and the ionized gas. In all of the four objects studied here, the electron densities deduced from the [N I]

doublet agree well with those deduced from the [S II] and [Cl III] doublet ratios that were also observed by us (Table 4).

4 DISCUSSION

4.1 Excitation mechanisms for the [C I] lines: collisions versus recombination

Before the [C I] far-red forbidden line fluxes can be used for diagnostic purposes, it is essential to establish their dominant excitation mechanism.

Via detailed modelling calculations of the thermal structure and chemistry of partially ionized envelopes of dense molecular clouds exposed to intense stellar radiation fields longwards of the H I Lyman limit, Escalante et al. (1991) showed that the [C I] far-red forbidden lines observed from M 42 and NGC 2024 can be interpreted as emission arising from gas with hydrogen densities in excess of 10^5 cm^{-3} exposed to radiation fields with intensities between 10^3 and 10^6 times the average diffuse interstellar radiation field. Radiative recombination of C^+ ions produced by photoionization was found to dominate the excitation of the [C I] lines, with only a negligible contribution from collisional excitation by electron impacts. Escalante et al. suggest that the [C I] emission observed from NGC 7027 (Danziger & Goad 1973) and NGC 6720 (Jewitt et al. 1983) may also originate from similar regions, with radiative recombination dominating the excitation. On the other hand, both Danziger & Goad (1973) and Jewitt et al. (1983) interpreted their data assuming collisional excitation.

The dominant excitation mechanism of the [C I] lines can be established by measuring the intensity ratio $I(\lambda9824+\lambda9850)/I(\lambda8727)$, which has quite different values under collisional excitation and radiative recombination excitation. Fig. 2 shows the variation of this ratio as a function of electron temperature T_e for pure radiative recombination (solid lines) and pure collisional excitation (dashed lines). The effective recombination coefficients of C^0 are taken from Escalante & Victor (1990). The results for both case A and case B are plotted. In case A, all the transitions are assumed optically thin, whereas in case B all resonance transitions terminating in the ground state are prohibited. For collisional excitation, the line ratio was calculated using EQUIB, written originally by I. D. Howarth and developed by S. Adams. The transition probabilities were taken from Nussbaumer & Rusca (1979) and collisional strengths from Thomas & Nesbet (1975) and Péquignot & Aldrovandi (1976). Three curves, corresponding to electron densities of $N_e = 10^3$, 10^4 and 10^5 cm^{-3}, are shown.[1] For collisional excitation, the line ratio is also quite sensitive to the electron density, due to the relatively low critical density of the $2p^2\,{}^1D$ level from which the 9824- and 9850-Å transitions originate, $\sim 4.8\times10^4$, 2.2×10^4 and 1.6×10^4 cm^{-3} for $T_e = 1000$, 5000 and 10 000 K, respectively. At densities higher than 10^4 cm^{-3}, the ^1D level population is quenched by electron impacts, decreasing the line ratio. This implies that

[1]In this paper, we neglect collisional excitation by H^+, H^0 and He^0 impacts. Although these processes can be important in exciting the fine-structure levels of the ground term ^3P, they are not important for the $^1D_2$ and $^1S_0$ levels considered here. A detailed analysis of populations of the O^0 metastable levels including these collisional processes is presented by Péquignot (1990).

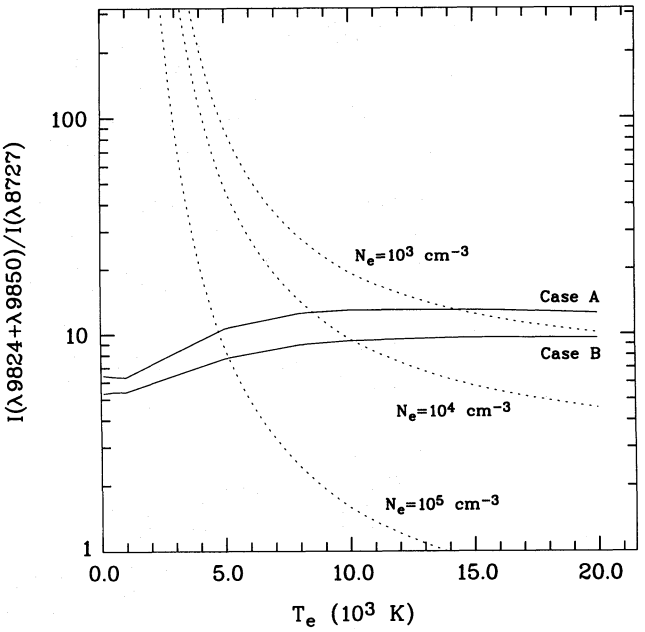

Figure 2. The [C I] forbidden line ratio $I(\lambda9824+\lambda9850)/I(\lambda8727)$ as a function of electron temperature T_e for radiative recombination excitation (solid lines) and collisional excitation by electron impacts (dashed lines). See text for details.

the curves given in Fig. 2 for pure radiative recombination excitation are actually upper limits for possible line ratios. At finite densities, the line ratio can be smaller than predicted by the solid curves, even if radiative recombination dominates the excitation. In the PDR models of Escalante et al. (1991), the [C I] lines arise from regions with electron temperatures ranging from a few hundred K up to 1000 K, yielding line ratios that fall in a narrow range between 6 and 9 for $N(H+2H_2) = 10^3$–10^7 cm^{-3} and radiation field enhancement factors $\chi = 10$–10^6.

A comparison between Fig. 2 and the observed $I(\lambda9824+\lambda9850)/I(\lambda8727)$ ratios listed in Table 3 shows clearly that radiative recombination cannot be the dominant excitation mechanism for the [C I] emission observed in three of the PNe. Instead, the observed line ratios are characteristic of collisional excitation. With the exception of NGC 2440, the nebulae all have line ratios around 30, a factor of 3 larger than those predicted by recombination theory. As described in Section 1, previous detections of [C I] emission from PNe included NGC 7027 (Danziger & Goad 1973) and NGC 6720 (Jewitt et al. 1983). In both cases, the $\lambda8727$ line was not detected directly. For NGC 7027, Danziger & Goad gave a line ratio of 3.5 from an estimate of the intensity of the $\lambda8727$ line obtained by comparing the observed intensity of the hydrogen P 12 line, blended with the $\lambda8727$ line on their low-resolution spectrogram, with its predicted value from recombination theory. For NGC 6720, Jewitt et al. gave an upper limit to the intensity of the $\lambda8727$ line such that $I(\lambda9824+\lambda9850)/I(\lambda8727) > 14$.

Collisional de-excitation of the ^1D level by electron impacts is clearly responsible for the very small [C I] line ratio apparently observed in NGC 7027, which is one of the densest PNe known, with an N_e between 35 000 and 80 000 cm^{-3} (e.g. Keyes, Aller & Feibelman 1990; Middlemass 1990). The same process may also be responsible for the low

ratio of 9.5 observed in NGC 2440, close to the predictions of recombination theory. However, as listed in Table 4, the electron density of NGC 2440 deduced from several different density diagnostics, including the [N I] doublet, is only a few $\times 10^3$ cm^{-3}. On the other hand, NGC 2440 has a very complex structure, with many knots and filaments (see the *HST* image taken in the [N I] lines and adjacent continuum presented by Heap 1993). It is possible that the observed [C I] line emission arises mainly from partially ionized dense knots or condensations.

However, another possibility to explain the small line ratio observed in NGC 2440 is that, in this particular object, recombination makes a significant or even dominant contribution to the observed flux. The importance of recombination in exciting the observed [C I] lines can be established by searching for C I recombination lines arising from much higher excitation energy levels and which cannot therefore be excited by collisional excitation. For this purpose, we have searched the effective recombination coefficient tables for C I calculated by Escalante & Victor (1990). The three optically permitted multiplets with the largest effective recombination coefficients are C I M 3 $3p\,^3P$–$3s\,^3P^o$ at 9089 Å, M 2 $3p\,^3S$–$3s\,^3P^o$ at 9642 Å and M 26 $4d\,^3F^o$–$3p\,^3D$ at 7116 Å. Of the three multiplets, M 2 falls in a wavelength region crowded by telluric absorption lines and is thus useless. The strongest component of M 3 (J=2–2) has a rest wavelength of 9094.289 Å. For NGC 2346, NGC 3132 and IC 4406, this line is seriously affected by water vapour absorption. Fortunately, for NGC 2440, the relatively large positive nebular radial velocity redshifts this line to 9096.09 Å, taking it clear of absorption (the blue component of the λ9094.289 line may possibly be affected by the nearest water vapour absorption line at 9095.369 Å given an expansion velocity of 33 km s^{-1} (Swensson et al. 1970; Meatheringham et al. 1988)). The spectrum of NGC 2440 showing this wavelength region is shown in Fig. 3. Assuming pure radiative recombination excitation, the predicted wavelength and intensity of the λ9094.289 line, as estimated from the observed intensity of the λ8727 line using the effective recombination coefficients of Escalante & Victor (1990), are plotted in Fig. 3 for three cases: (a) the effective recombination coefficients of both the λ8727 and λ9094.289 lines follow case A; (b) both lines follow case B; (c) the effective recombination coefficient of the [C I] λ8727 line follows case A, whereas that of the C I λ9094.289 line follows case B. Here an electron temperature of T_e=5000 K has been assumed. The intensity ratio of the λ9094.289 and the λ8727 lines depends only weakly on temperature. For example, the intensity ratio decreases by less than 10 per cent for T_e=8000 K and increases by less than 40 per cent for T_e=1000 K. As can be seen in Fig. 3, the observed spectrum of NGC 2440 does show a weak feature with a S/N ratio about 2.5 at nearly the expected wavelength of the λ9094.289 line. Unfortunately, the predicted intensity of the

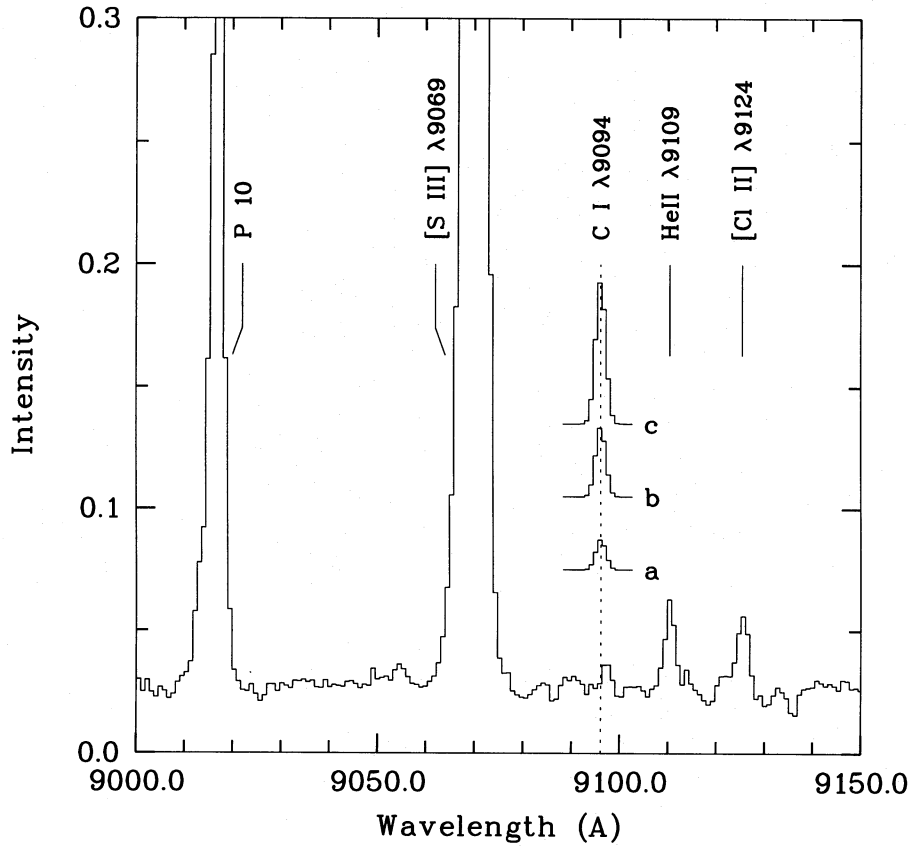

Figure 3. The spectrum of NGC 2440 between 9000 and 9150 Å. Assuming radiative recombination, the line profiles overplotted show the predicted wavelength and intensities of the C I λ9094 line of M 3 for three cases: (a) both λ8727 and λ9094 lines are in case A; (b) both are in case B; (c) the λ8727 line obeys case A, whereas the λ9094 line obeys case B. The spectrum is normalized such that $I(H\beta)$=100. See text for details.

λ9094.289 line depends strongly on the optical thickness assumption. The observation would agree roughly with the prediction of recombination theory if the effective recombination coefficients of both the λ8727 and the λ9094.289 lines obeyed case A. Since the ground level of C^0 ($2p^2\,^3P$) is a triplet, and the λ8727 and λ9094.289 lines arise from singlet and triplet states, respectively, by analogy with the well-studied O II recombination spectrum (Liu et al. 1995), we expect the effective coefficient of the λ8727 line to be given by case A, whereas that of the λ9094.289 line should be given by case B. If this is the case, then the contribution from radiative recombination to the observed λ8727 line flux should be less than 20 per cent. On the other hand, the column density of C^0 ions depends not only on the ionization structure of the nebula but also on the chemistry of the neutral envelope surrounding it. Here the carbon abundance may also be important. In this context it may be relevant to note that NGC 2440 is carbon-deficient (e.g. Shields et al. 1981). At the moment, it is difficult to estimate the optical depth of C I resonance lines without detailed calculations of the ionization *and* chemistry of the nebula. In this context, submillimetre observations of the [C I] fine structure lines at 369 and 609 μm could be invaluable.

A way to distinguish between these various possibilities is to observe lines from the C I M 26 multiplet near 7116 Å. The strongest component of this multiplet, λ7113.180 ($J=4$–3), has an intensity relative to the [C I] λ8727 line of 0.109, 0.0559 and 0.114 at $T_e=5000$ K for the three cases (a), (b) and (c) listed above. Though weaker than the λ9094.289 line, the λ7113.180 line has the great advantage that it falls in a region unaffected by telluric absorption and also lies where CCD chips have much higher quantum efficiencies. Most importantly, the effective recombination coefficient of M 26 is almost independent of the optical thickness: its emissivity changes by less than 5 per cent from case A to case B. Thus, by comparing this line with the λ9094.289 line, it should be possible to establish whether the triplet C I lines obey case A or case B. Unfortunately, the λ7113.180 line fell outside our observing window. A further search for this line from NGC 2440 would be very useful, as it can be used to derive the C^+ abundance. With modern, high quantum efficiency CCDs, when observed at a medium–high resolution (say 0.3 Å pixel^{-1}), lines with intensities as weak as 0.01, in units where $H\beta=100$, can be reached with modest effort (Liu et al. 1995).

The [C I] lines from NGC 2440 are the weakest amongst the four nebulae observed: the intensity of the λ9850 line relative to Hβ is about 4 to 10 times weaker than for the other objects. This may reflect the fact that NGC 2440 is carbon-deficient. However, it is worthwhile noting that the H_2 emission from NGC 2440 is also the weakest amongst the four objects in our sample. The contribution made by radiative recombination to the [C I] line fluxes observed in the other three nebulae, NGC 2346, NGC 3132 and IC 4406, should be small, since the [C I] line fluxes from these objects are much stronger than those from NGC 2440.

4.2 Fluorescent excitation

A number of UV intercombination resonance absorption lines of neutral carbon have been observed in lines of sight to hot stars passing through diffuse interstellar clouds (e.g. Morton 1975, 1991). This raises the possibility that the [C I] lines observed here could be excited by stellar continuum fluorescence. However, we will show below that this process is negligible for the objects of interest here.

Bound–bound radiative transition probabilities for C I have been calculated by Nussbaumer & Storey (1984) and by Luo & Pradhan (1989). Since neutral carbon can be photoionized by radiation shortwards of 1101 Å, it is reasonable to assume that in the C^0 region only radiation longwards of 1101 Å is abundant. Possible pumping routes that lead to excitation of the singlet levels $2p^2\,^1D$, ^1S include the intercombination transitions $2p^2\,^3P$–$nl\,^1L^0$, where $n\geq 3$, l = s, p, d, and L = P, D, F. These transitions all fall between 1110 and 1614 Å (Morton 1991).

First of all, we note that UV fluorescence cannot be the dominant excitation mechanism for the [C I] emission observed from these PNe. Following the absorption of an intercombination line photon, the excited C^0 atom will eventually cascade down to the ground electron configuration, with probabilities of 1/6 and 5/6 respectively of terminating at the $2p^2\,^1S$ and ^1D levels. Using the [C I] transition probabilities calculated by Nussbaumer & Rusca (1979), it can be shown that, of the 1/6 pumped C^0 atoms that cascade down to the $2p^2\,^1S$ level, 99.5 per cent of them terminate at the ground term $2p^2\,^3P$ via the $2p^2\,^1S$–$2p^2\,^1D$ transition; only 0.5 per cent of them decay directly to the ground term via the $2p^2\,^1S$–$2p^2\,^3P$ transition. Therefore, under pure fluorescence conditions, we expect a line ratio $R\equiv I(\lambda 9824+\lambda 9850)/I(\lambda 8727)\simeq 6\times 8727/9840=5.3$, similar to the values predicted under pure radiative recombination and much smaller than those observed.

The [C I] λλ9824, 9850 lines observed from the four PNe studied here are so strong that any contamination by stellar continuum fluorescence can be safely neglected. For the much weaker λ8727 line, an upper limit on the possible contamination from this process can be obtained from energy considerations. The luminosity of the λ8727 line produced by fluorescent excitation of an intercombination line of frequency ν and equivalent width w_ν is given by $Bw_\nu L_\nu^* E(\lambda 8727)/h\nu$, where B is the probability of emitting a λ8727 photon of energy $E(\lambda 8727)$ following fluorescent pumping, and L_ν^* is the stellar monochromatic luminosity at frequency ν. We estimate that $B=1/6=0.167$. For an optically thick line, w_ν will be a few Doppler widths. For the PNe of interest here, it is likely that most of the C I intercombination lines are optically thin. For comparison, the diffuse clouds towards ζ Ophiuchi have a total colour excess of $E(B-V)=0.32$, a total H column density of $N(H+2H_2)=1.3\times 10^{21}$ cm^{-2} and a C^0 column density of $N(C^0)=3.6\times 10^{15}$ cm^{-2}, while the strongest C I intercombination lines observed towards ζ Ophiuchi have an equivalent width of about 25 mÅ (Morton 1975). All four of the PNe observed here have a colour excess less than that of ζ Ophiuchi, and it is reasonable to assume that the C^0 column densities in these PNe are much smaller than that observed towards ζ Ophiuchi. Taking the C^0 intercombination absorption lines observed towards ζ Ophiuchi (Morton 1975) as a reference, we estimate that the maximum luminosity of the [C I] λ8727 line that can be produced by UV fluorescent excitation, $L_f(\lambda 8727)$, is given by

$$L_f(\lambda 8727)\leq 20B\nu_D\frac{\pi B_\nu}{\sigma T_{\rm eff}^4}\frac{E(\lambda 8727)}{h\nu}L^*, \qquad (1)$$

equivalent to a $\lambda 8727$ luminosity produced by pumping by 20 intercombination lines, each of them having an equivalent width of $w_\nu = \nu_D = 2(\ln 2)^{1/2}(2kT_e/Am_p)^{1/2}$ (~ 25 mÅ for $T_e = 10^4$ K and $\lambda = c/\nu = 1200$ Å, the same as the largest equivalent width for the C I intercombination lines observed towards ζ Ophiuchi). Here ν_D is the FWHM of the Doppler line profile, and $A = 12$ is the atomic weight of carbon. In equation (1), we have assumed that the PN central star emits as a blackbody with an effective temperature of $T_{\rm eff}$ and a total luminosity of L^*. Inserting numerical values into equation (1) we get

$$L_f(\lambda 8727) \leq \frac{2.6\times 10^{-7}}{\lambda^3 T_{\rm eff}^4} T_e^{1/2} (e^{1.44/\lambda T_{\rm eff}} - 1)^{-1} L^*, \qquad (2)$$

where λ is in units of 1000 Å, $T_{\rm eff}$ is in units of 10^5 K, and T_e is in units of 10^4 K.

The properties of the central stars of the PNe in our sample are summarized in Table 5, where columns 2–5 give the adopted distance, effective temperature, luminosity and references for these quantities. The estimated maximum luminosity of the $\lambda 8727$ line that can be produced by stellar continuum fluorescence as calculated from equation (2) is given in column 6. A typical wavelength of $\lambda = 1200$ Å for the pumping intercombination lines was assumed. The observed luminosities are listed in the last column. Solid angles of 3.88×10^{-8}, 1.27×10^{-8}, 3.33×10^{-8} and 2.18×10^{-8} sr, for the [C I] emitting areas of NGC 2346, NGC 2440, NGC 3132 and IC 4406, respectively, were used to calculate $L_{\rm obs}(\lambda 8727)$ from the surface brightnesses listed in Table 3. These solid angles were estimated from the extent of the [C I] emission lines on our long-slit spectra. NGC 2346 and 3132 are binary systems, each consisting of an A-type main-sequence star and a hot subdwarf companion (e.g. Mendez 1978). For these two nebulae, contributions to $L_f(\lambda 8727)$ from both stars of the binary system are listed. In both cases, the contribution from the cool primary star is negligible compared to that from its hot companion.

Comparison between the values of $L_f(\lambda 8727)$ and $L_{\rm obs}(\lambda 8727)$ listed in Table 5 shows that stellar continuum fluorescence fails to reproduce the observed luminosities of the [C I] $\lambda 8727$ line from NGC 2346, NGC 2440, NGC 3132 and IC 4406, by factors of 28, 107, 15 and 48, respectively. We therefore conclude that UV continuum fluorescence is negligible in exciting the [C I] far-red forbidden lines observed from the four PNe studied here. Note that the values of $L_{\rm obs}(\lambda 8727)$ listed in Table 5 were derived using the same distances used for the calculation of L^*, so our conclusion is independent of the distances assumed.

4.3 Electron temperatures derived from the [C I] line ratios

We have shown that the observed [C I] line ratios are consistent with collisional excitation by electron impacts and UV fluorescence and radiative recombination are unimportant in exciting these lines, with the possible exception of NGC 2440 where a contribution from radiative recombination cannot be ruled out. As described in Section 1, C^0 has the same ground configuration as O^{2+}, so in the case of collisional excitation the observed [C I] line ratio, $R \equiv I(\lambda 9824 + \lambda 9850)/I(\lambda 8727)$, like the [O III] line ratio $I(\lambda 4959 + \lambda 5007)/I(\lambda 4363)$, provides a direct diagnostic of the electron temperature. However, due to the relatively low critical density of the C^0 ^1D level, at densities higher than 10^4 cm^{-3} the ratio R becomes increasingly sensitive to the electron density as well. The variation of R as a function of electron temperature T_e, for electron densities $N_e = 10^3$, 10^4 and 10^5 cm^{-3}, has been shown in Fig. 2.

The electron densities deduced from several different density diagnostics are given in Table 4, including those from the [N I], [S II] and [Cl III] doublets, in order of increasing ionization degree. In all cases, the densities deduced from the three diagnostics are in close agreement with each other. In particular, there is no evidence that the densities deduced from diagnostics from lower ionization species are larger than those from diagnostics from higher ionization species (in IC 4406, there is evidence that the density does increase toward lower ionization regions, but the changes are quite small). The N^0 and C^0 atoms have ionization potentials of 14.534 and 11.260 eV, respectively, and the upper levels of the [N I] $\lambda\lambda 5198$, 5200 doublet, the [C I] $\lambda\lambda 9824$, 9850 doublet and the [C I] $\lambda 8727$ line have excitation energies of 2.38, 1.26 and 2.68 eV, respectively. Given the similar ionization potentials as well as line excitation energies, the electron densities derived from the observed [N I] $\lambda\lambda 5198$, 5200 doublet ratios should be representative of the [C I] emitting regions. The electron temperatures deduced from the [C I] line ratio R using the electron density derived from the [N I] ratio are presented in Table 4. The temperature deduced in this way for NGC 2440 seems too high as compared to those derived from the [O I] and [N II] lines. As

Table 5. Fluorescence excitation of the [C I] $\lambda 8727$ line.

Object	D (pc)	T_{eff} (10^5 K)	L^* ($L_\odot$)	Ref	$L_f(\lambda 8727)$ ($L_\odot$)	$L_{obs}(\lambda 8727)$ ($L_\odot$)
NGC 2346	500	.080	14	(1),(2)	3.2×10^{-7}	6.1×10^{-4}
		1.00	17		2.2×10^{-5}	
NGC 2440	2190	2.00	2100	(6),(7)	5.7×10^{-4}	6.1×10^{-2}
NGC 3132	600	.095	50	(1)	6.0×10^{-6}	1.8×10^{-3}
		0.90	72		1.2×10^{-4}	
IC 4406	1600	0.94	170	(4),(5)	2.5×10^{-4}	1.2×10^{-2}

References: (1) Mendez (1978); (2) Walsh (1983); (3) Mendez & Niemela (1981); (4) Sahai et al. (1991); (5) Kaler & Jacoby (1989); (6) Heap & Hintzen (1990); (7) Gathier, Pottasch & Pel (1986).

described above, the low [C I] line ratio observed in NGC 2440 is difficult to understand from collisional excitation alone, unless the density is much higher than those listed in Table 4. For example, if we assume $T_e([C\,I]) = T_e([O\,I]) = 9830$ K (Section 3.3), then the observed [C I] line ratio implies an electron density of 1.05×10^4. This density is, however, not unrealistic, given the extremely complex structure of this object (see the *HST* image in the [N I] lines, Heap 1993).

The electron temperatures derived from the [C I] lines emitted by NGC 2346, NGC 3132 and IC 4406 are all systematically lower, by about 1800 to 2800 K, than those derived from the [N II] or [O III] line ratios, reflecting the general drop of temperature expected on going from the ionized region through the transition region to the neutral envelopes surrounding the nebulae. The temperatures are, however, much higher than those predicted by the standard PDR models (e.g. Tielens & Hollenbach 1985; Escalante et al. 1991). Obviously, the PDR models that have been developed for diffuse interstellar clouds and the dense molecular envelopes surrounding young H II regions may not be directly applicable to the warm neutral envelopes and ionization transition regions surrounding the PNe observed here. In the standard Galactic PDR regions, the gaseous nebulae are photoionized and heated by OB stars which have effective temperatures between 20 000 and 30 000 K. Their ionizing radiation fields peak near the ionizing thresholds of H^0 and C^0. In contrast, for the PNe studied here, the nebulae are excited by much harder radiation fields emitted by their much hotter central stars. With the exception of NGC 2440, the central stars of the nebulae in our sample also have quite low luminosities (Table 5). The Galactic PDRs would therefore be exposed to very large photon fluxes in the C^0 ionizing continuum between 912 and 1101 Å, while the PNe observed here would not. It is possible that, under such circumstances, a significant transition zone of relatively high electron temperature could exist in the PNe, where H^0, H^+ (and hence e^-), C^0, N^0, O^0 and S^+ co-exist. This may explain why in the standard PDRs, such as those found in M 42 and NGC 2024, the [C I] far-red forbidden lines appear to be excited by radiative recombination, whereas in PNe such as those studied here these lines are dominated by collisional excitation by electron impacts. This interpretation can be tested by detailed modelling calculations. However, to model successfully the warm transition zone and neutral regions observed in these PNe, a treatment of the thermal and ionization structure and of the radiative transfer in the neutral zones, transition regions and ionized main parts of the nebulae is required. Such calculations could be invaluable, but are beyond the scope of the current paper.

Of the four nebulae observed here, a common feature of three of them, NGC 2346, NGC 3132 and IC 4406, is that they all show extraordinarily strong molecular emission. In addition to H_2 and CO, species such as HCN, HNC, HCO^+ and CN have also been observed (Storey 1984; Zuckerman & Gatley 1988; Bachiller et al. 1989; Sahai, Wootten & Clegg 1990; Sahai et al. 1991; Cox et al. 1992). One of the goals of the observations carried out here was to provide constraints on the physical conditions prevailing in the warm neutral zones and transition regions surrounding PNe, where the infrared H_2 lines originate. Recently, we have obtained deep, high-resolution *K*-band spectra of the molecular hydrogen emission lines emitted by NGC 2346 and 3132. The results presented here on the two nebulae will be discussed further in a separate paper, where we will present our near-infrared data on the H_2 emission lines (Liu et al., in preparation).

5 SUMMARY

We have obtained the first measurements of the [C I] far-red forbidden line ratio, $I(\lambda 9824 + \lambda 9850)/I(\lambda 8727)$, in the planetary nebulae NGC 2346, NGC 2440, NGC 3132 and IC 4406. The observed line ratios are consistent with collisional excitation by electron impacts. We have shown that stellar continuum fluorescence and radiative recombination are unimportant in exciting these lines, with the possible exception of NGC 2440 where a contribution from radiative recombination cannot be ruled out. For NGC 2346, NGC 3132 and IC 4406, the observed line ratios yield electron temperatures in the range 7400 to 8000 K.

ACKNOWLEDGMENTS

We thank Dr D. Péquignot for providing the identification of the He II λ9109 line shown in Fig. 3. IRAF is distributed by National Astronomy Observatories, which is operated by the Association of Universities for Research in Astronomy, Inc., under contract to the National Science Foundation.

REFERENCES

Bachiller R., Planesas P., Martin-Pinado J., Bujarrabal V., Tafalla M., 1989, A&A, 210, 366
Burton M. G., Bulmer M., Moorhouse A., Geballe T. R., Brand P. W. J. L., 1992, MNRAS, 257, 1P
Butler K., Dalgarno A., 1979, ApJ, 234, 765
Clegg R. E. S., Harrington J. P., Barlow M. J., Walsh J. R., 1987, ApJ, 314, 551
Cox P., Omont A., Huggins P. J., Bachiller R., Forveille T., 1992, A&A, 266, 420
Dalgarno A., 1978, in Terzian Y., ed., Proc. IAU Symp. 76, Planetary Nebulae. Kluwer, Dordrecht, p. 23
Danziger I. J., Goad L. E., 1973, Astrophys. Lett., 14, 115
Delbouille L., Roland G., 1963, Photometric Atlas of the Solar Spectrum from λ7498 to λ12016. Mem. Soc. R. Sci. Liège, Spec. Vol. No. 4
Escalante V., Victor G. A., 1990, ApJS, 73, 513
Escalante V., Sternberg A., Dalgarno A., 1991, ApJ, 375, 630
Gathier R., Pottasch S. R., Pel J. W., 1986, A&A, 157, 171
Heap S. R., 1993, in Weinberger R., Acker A., eds, Proc. IAU Symp. 155, Planetary Nebulae. Kluwer, Dordrecht, p. 23
Heap S. R., Hintzen P., 1990, ApJ, 353, 200
Hippelein H., Münch G., 1978, A&A, 68, 17
Huggins P. J., 1993, in Weinberger R., Acker A., eds, Proc. IAU Symp. 155, Planetary Nebulae. Kluwer, Dordrecht, p. 147
Hummer D. G., Storey P. J., 1987, MNRAS, 224, 801
Jewitt D. C., Kupferman P. N., Danielson G. E., Maran S. P., 1983, ApJ, 268, 683
Kaler J. B., Jacoby G. H., 1989, ApJ, 345, 871
Kaufman V., Sugar J., 1986, J. Phys. Chem. Ref. Data, 15, 321
Keyes C. D., Aller L. H., Feibelman W. A., 1990, PASP, 102, 59
Lambert D. L., Swings J. P., 1967, Sol. Phys., 2, 34
Liu X. W., Danziger I. J., 1993, MNRAS, 261, 465
Liu X. W., Storey P. J., Barlow M. J., Clegg R. E. S., 1995, MNRAS, 272, 369
Luo D., Pradhan A. K., 1989, J. Phys. B: At. Mol. Opt. Phys., 22, 3377

Meatheringham S. J., Wood P. R., Faulkner D. J., 1988, ApJ, 334, 862
Mendez R. H., 1978, MNRAS, 185, 647
Mendez R. H., Niemela V. S., 1991, ApJ, 250, 240
Mendoza C., 1983, in Flower D. R., ed., Proc. IAU Symp. 103, Planetary Nebulae. Kluwer, Dordrecht, p. 143
Mendoza C., Zeippen C. J., 1982, MNRAS, 199, 1025
Middlemass D., 1990, MNRAS, 244, 294
Moore C. E., 1972, A Multiplet Table of Astrophysical Interest, NBS No. 40
Morton D. C., 1975, ApJ, 197, 85
Morton D. C., 1991, ApJS, 77, 119
Münch G., Hippelein H., 1982, Ann. N.Y. Acad. Sci., 395, 170
Nussbaumer H., Rusca C., 1979, A&A, 72, 129
Nussbaumer H., Storey P. J., 1984, A&A, 140, 383
Oke J. B., 1974, ApJS, 27, 21
Oke J. B., 1990, AJ, 99, 162
Osterbrock D. E., Martel A., 1992, PASP, 104, 76
Osterbrock D. E., Tran H. D., Veilleux S., 1992, ApJ, 389, 305
Péquignot D., 1990, A&A, 231, 499
Péquignot D., Aldrovandi S. M. W., 1976, A&A, 50, 141
Reay N. K., Walton N. A., Atherton P. D., 1988, MNRAS, 232, 615
Richer M. G., McCall M. L., Martin P. G., 1991, ApJ, 377, 210
Sahai R., Wootten A., Clegg R. E. S., 1990, A&A, 234, L1
Sahai R., Wootten A., Schwarz H., Clegg R. E. S., 1991, A&A, 251, 560
Schneider S. E., Terzian Y., Purgathofer A., Perinotto M., 1983, ApJS, 52, 399
Seaton M. J., 1979, MNRAS, 187, L73
Shields G. A., Aller L. H., Keyes C. D., Czyzak S. J., 1981, ApJ, 248, 569
Stafford R. P., Bell K. L., Hibbert A., Wijesundera W. P., 1994, MNRAS, 268, 816
Stevenson C. C., 1994, MNRAS, 267, 904
Storey J. W. V., 1984, MNRAS, 206, 521
Swensson J. W., 1967, Naturwissenschaften, 54, 440
Swensson J. W., Benedict W. S., Delbouille L., Roland G., 1970, The Solar Spectrum from λ7498 to λ12016. A Table of Measures and Identifications. Mem. Soc. R. Sci. Liège, Spec. Vol. No. 5
Thomas L. D., Nesbet R. K., 1975, Phys. Rev. A, 12, 2378
Tielens A. G. G. M., Hollenbach D., 1985, ApJ, 291, 722
Torres-Peimbert S., Peimbert M., 1977, Rev. Mex. Astron. Astrofis., 2, 181
Walsh J. R., 1983, MNRAS, 202, 303
Walsh J. R., 1993, ST-ECF Newsl., 19, 6
Walsh J. R., Meaburn J., Whitehead M. J., 1991, A&A, 248, 613
Zuckerman B., Gatley I., 1988, ApJ, 324, 501

APPENDIX A: DETERMINATION OF THE [S III] ELECTRON TEMPERATURE

The observed intensities of the [S III] nebular lines at 6312.1, 9068.9 and 9531.0 Å, after reddening corrections, are given in Table A1. The intensities are normalized such that $I(\mathrm{H}\beta)=100$, via either Hα or P11 (Section 3). The last two columns of Table A1 give the [S III] nebular-to-auroral line ratio $I(\lambda9069+\lambda9531)/I(\lambda6312)$ (see below) and the electron temperature deduced from it. The transition probabilities and collision strengths for [S III] were taken from Mendoza & Zeippen (1982) and Mendoza (1983), respectively.

At a resolution of 2 Å (FWHM), [S III] λ6312.1 is blended with the He II 16 ^{2}H^o–5 ^{2}G (M 7) line at 6310.80 Å. To correct for the contribution from the latter, we have made use of the He II 7 ^{2}G–4 ^{2}F^o (M 2) line at 5411.52 Å. At the temperatures and densities relevant here, He II λ6311/λ5411 = 0.0458, derived from case B recombination theory (Hummer & Storey 1987). The dereddened intensities of the λ5411 line from our spectra are 1.42, 5.70, 0.14 and 1.14, in units where $\mathrm{H}\beta=100$, for NGC 2346, NGC 2440, NGC 3132 and IC 4406, respectively. The dereddened intensities of the [S III] λ6312 line listed in Table A1 have been corrected for contamination from the He II λ6311 line. The weakness of the He II λ5411 line in NGC 3132 is mainly due to the fact that we excluded an area 26.24 arcsec in length centred on the central star when integrating the spectra along the slit (cf. Section 3.2). This was done for the spectra covering both the 5023–7007 and 8010–9980 Å wavelength ranges.

The [S III] λλ9069, 9531 lines fall in wavelength regions crowded by water vapour absorption lines. Recently, Stevenson (1994) has developed a sophisticated method to correct for the effects of telluric absorption by numerically modelling the telluric absorption lines. However, due to the complexity of the problem and the presence of many possible factors that can change the actual level of absorption, only limited success has been achieved using this method. Here we rely on the simple method we used in Section 3.2 in connection with our discussion of the [C I] lines by checking whether the line concerned is affected by telluric absorption lines, given the known radial and expansion velocities. As described in Section 2, instead of dividing the raw spectra by the calibration spectra pixel by pixel to correct for instrumental response and telluric absorption, we flux-calibrated our spectra using an instrumental monochromatic response curve deduced by fitting with a smooth curve the calibration points known to be unaffected by telluric absorption. In this way we have avoided one of the major sources of error discussed by Stevenson (1994). Note that, following the recommendation of Osterbrock, Tran & Veilleux (1992), we have adopted the new rest wavelengths of 6312.1, 9068.9 and 9531.0 Å for the [S III] forbidden lines, as given by Kaufman & Sugar (1986), instead of the old values of 6310.2, 9069.4 and 9532.1 Å from the RMT (Moore 1972). The wavelengths of the λλ9069, 9531 lines are still quite uncertain, with a quoted error of 0.7 Å in Kaufman & Sugar (1986). The comments on individual objects given below are quite sensitive to the rest wavelengths adopted for the [S III] forbidden lines.

In the vicinity of the [S III] λλ9069, 9531 lines, prominent water vapour absorption lines include ones at 9069.126, 9071.958, 9529.440, 9531.226, 9531.726 and 9533.411 Å

Table A1. [S III] line fluxes from four planetary nebulae.[a]

Object	λ6312	λ9069	λ9531	R[b]	T_e (K)
NGC 2346	.465	10.4	26.7	79.8	9150
NGC 2440	1.69	13.2	34.52:	27.2	15640
NGC 3132	2.45	50.2	126.:	71.3	9560
IC 4406	.642	10.8	10.6:	58.6	10360

[a]Measurements possibly affected by telluric absorption are marked by a colon.
[b]$R \equiv I(\lambda9069+\lambda9531)/I(\lambda6312)$. If one of the λλ9069, 9531 lines is affected by telluric absorption, only the line clear of telluric absorption is used to calculate R. The other line is incorporated assuming $I(\lambda9531)/I(\lambda9069)=2.48$ as derived from the transition probabilities given by Mendoza & Zeippen (1982).

(Delbouille & Roland 1963; Swensson et al. 1970). In Section 3.2, we assumed that a measurement could be affected by telluric absorption if there were one or more telluric absorption lines with central optical depths in excess of 0.2, as seen on the solar spectrum atlas of Delbouille & Roland (1963), falling within the range $\lambda^{\rm Earth}(1-\Delta V/c)$ to $\lambda^{\rm Earth}(1+\Delta V/c)$, where $\lambda^{\rm Earth}$ is the wavelength in the Earth reference frame of the line of interest, $\Delta V = V_{\rm exp} + V_{\rm D}$ is the sum of the nebular expansion velocity and thermal Doppler width, and c is the velocity of light. For $T_{\rm e} = 10^4$K, $V_{\rm D} = 2.3$ km s^{-1} for sulphur. Values of $V_{\rm exp} = 12.0$, 33.0, 21.0 and 14.0 km s^{-1} were adopted for NGC 23546, NGC 2440, NGC 3132 and IC 4406, respectively (Section 3.2). Following these guidelines, we give below brief comments on the far-red [S III] forbidden line measurements for the four PNe studied here.

NGC 2346

The geocentric wavelength of [S III] λ9069 lies at 9070.05 Å, and the nearest water vapour line is 31 km s^{-1} bluewards. Similarly, the [S III] λ9531 line has a geocentric wavelength of 9532.21 Å, with the nearest water vapour line 15 km s^{-1} bluewards. Thus both lines are likely to be free of serious telluric absorption. The measured line intensities give a ratio $I(\lambda9531)/I(\lambda9069) = 2.58$, in close agreement with the theoretical value of 2.48 deduced from the transition probabilities of Mendoza & Zeippen (1982). The derived temperature is, however, slightly lower compared to those derived from the [N II] and [O III] lines (Table 2). One possibility is that reddening toward this nebula has been slightly underestimated.

NGC 2440

The nearest water vapour absorption line, at 9071.958 Å, falls 42 km s^{-1} redwards of the [S III] λ9069 line. However, the λ9531 line is only 16 km s^{-1} bluewards of the water vapour line at 9533.411 Å. The line ratio R and the resultant $T_{\rm e}$ listed in Table A1 were calculated using the λ9069 line only. The contribution from the λ9531 line is taken into account assuming $I(\lambda9531)/I(\lambda9069) = 2.48$. However, given the small Doppler width of the [S III] lines, and provided that the turbulent velocities within the nebula are insignificant, the λ9069 line may not be affected by telluric absorption. In fact, our measurements give $I(\lambda9531)/I(\lambda9069) = 2.62$, not far from the theoretical value of 2.48.

NGC 3132

The [S III] λ9069 line is clear of telluric absorption, whereas the λ9531 line may be affected by the water vapour line at 9529.440 Å. The line ratio R and the resultant $T_{\rm e}$ listed in Table A1 were calculated using the λ9069 line only. The electron temperature deduced is in close agreement with those derived from the [N II] and [O III] lines.

IC 4406

Similarly to NGC 3132, the [S III] λ9069 line is clear of absorption, whereas the λ9531 line is seriously affected by water vapour lines crowded bluewards of 9529.440 Å. The line ratio R and the resultant $T_{\rm e}$ were calculated using the λ9069 line only.